The Time Programmable Frequency Comb: Generation and Application to Quantum-Limited Dual-Comb Ranging

Emily D. Caldwell[1], Laura C. Sinclair[1], Nathan R. Newbury[1], Jean-Daniel Deschenes[2]

[1]National Institute of Standards and Technology (NIST), Boulder, CO, USA

[2]Octosig Consulting, Quebec City, Canada

The classic self-referenced frequency comb acts as an unrivaled ruler for precision optical metrology in both time and frequency[1,2]. Two decades after its invention, the frequency comb is now used in numerous sensing applications[3–5]. Many of these applications, however, are limited by the tradeoffs inherent in the rigidity of the comb output and operate far from quantum-limited sensitivity. Here we demonstrate an agile programmable frequency comb where the pulse time and phase are digitally controlled with ±2 attosecond accuracy. This agility enables quantum-limited sensitivity in sensing applications since the programmable comb can be configured to coherently track weak returning pulse trains at the shot-noise limit. To highlight its capabilities, we use this programmable comb in a ranging system, reducing the required power to reach a given precision by ~5,000-fold compared to a conventional dual-comb system. This enables ranging at a mean photon per pulse number of 1/77 while retaining the full accuracy and precision of a rigid frequency comb. Beyond ranging and imaging[6–12], applications in time/frequency metrology[1,2,5,13–23], comb-based spectroscopy[24–32], pump-probe experiments[33], and compressive sensing[34,35] should benefit from coherent control of the comb-pulse time and phase.

As applications of frequency combs have expanded, their uses have extended beyond functioning simply as a reference ruler[3–5]. For example, many experiments combine two or more frequency combs for active sensing including precision ranging and imaging[6–12], linear and non-linear spectroscopy[24–32], and time transfer[13–20,23]. In these applications, the multiple fixed combs serve as differential rulers by phase-locking them to have a vernier-like offset between their frequency comb lines, or their pulses in time. While these applications exploit the accuracy and precision of frequency combs, they operate nowhere near the quantum (or shot noise) limit, despite the use of heterodyne detection, because of effective dead time due to sensing the incoming signal-comb light via a comb with a deliberately mismatched repetition frequency. Consequently, there are strong tradeoffs in measurement speed, sensitivity and resolution[24,36,37]. In some dual-comb ranging and spectroscopy demonstrations, these penalties have been partially addressed by incoherent modulation of the comb[38–41] but not eliminated.

Here, we overlay a self-referenced optical frequency comb with synchronous digital electronics for real-time coherent control of the comb's pulse train output. We manipulate the frequency comb's two phase locks to dynamically control and track the time and phase of the frequency comb's output pulses at will. The temporal placement of the comb pulses is set with ±2 attoseconds accuracy with a range limited only by slew rate considerations. This time programmable frequency comb (TPFC) goes beyond the "mechanical gear box" analogy often applied to optically self-referenced combs[5], replacing it with a digitally controllable, agile, coherent optical pulse source. The agility of the TPFC enables many more measurement modalities than a rigid frequency comb. In sensing applications, the TPFC can enable quantum-limited detection with the full accuracy and precision of the frequency comb, avoiding the penalties discussed previously. To achieve these combined advantages, the TPFC is configured as a tracking optical oscillator in time and phase so that it effectively locks onto an incoming weak signal pulse train for coherent signal integration.

As an immediate example, we incorporate the TPFC into a dual-comb ranging system. The result is quantum-limited sensing that sacrifices none of the exquisite accuracy and precision of frequency-comb measurements. Here, we show a precision floor of 0.7 nm (4.8 attoseconds in time-of-flight) in ranging, which exceeds previous conventional dual-comb ranging demonstrations[6–8,42–44]. In addition, the tracking dual-comb ranging detects a weak reflected signal-comb pulse-train with a mean photon number per pulse of only 1/77 at a sensitivity within a factor of two of the quantum limit. Detection of signals at even lower mean photon per pulse numbers is possible by reducing the measurement bandwidth. In contrast, conventional dual-comb ranging would require a return signal 37 dB or 5000x stronger to reach the same level of performance.

The uses of the TPFC go well beyond acting as a tracking optical oscillator. It should enable many more time-based measurement schemes than the conventional vernier approaches using fixed frequency combs. For example, in multi-comb sensing, the relative time offset between the frequency combs can be adjusted so as to mimic a higher repetition rate system while retaining the benefits of a lower repetition rate system, *e.g.* higher pulse energy and tight stabilization. Arbitrary patterns can enable future compressive sampling[35]. In time/frequency metrology, the comb can provide accurately adjustable timing signals, modulation capabilities for noise suppression, and optically-based time interval standards[45]. Multiple TPFCs could be used for pump-probe experiments with digital control of pulse spacing replacing delay lines or chirp-induced delays[33].

In this article, we first describe the TPFC and its capabilities generally. We then explore a specific application by integrating the TPFC into a dual-comb ranging system. Finally, we discuss the potential benefits of a TPFC in comb-based sensing more generally, including in LIDAR, spectroscopy, and time transfer.

RESULTS

Generation of a Time Programmable Frequency Comb

The TPFC requires two parts: an *optically* self-referenced frequency comb and the electronics to track and control the time and phase of the comb pulses. (See Methods Eqn. 3 for a definition of the time and phase of the comb pulses.) While the electronic system need not be exclusively digital, it does need to track the programmed comb time and phase at the attosecond level over long (hours to weeks) durations. Here, we use a fixed-point number whose least significant bit corresponds to < 1 attosecond shift in time. When combined with an integer pulse number in an 80-bit number, the pulse timing can be specified with zero loss of accuracy for over 1 week at 1-as precision, thereby providing well beyond 10^{19}-level control of the comb timing, commensurate with next-generation optical clocks. As for the comb, any self-referenced comb could be converted into a TPFC; here, we generate a TPFC using a fiber-based comb.

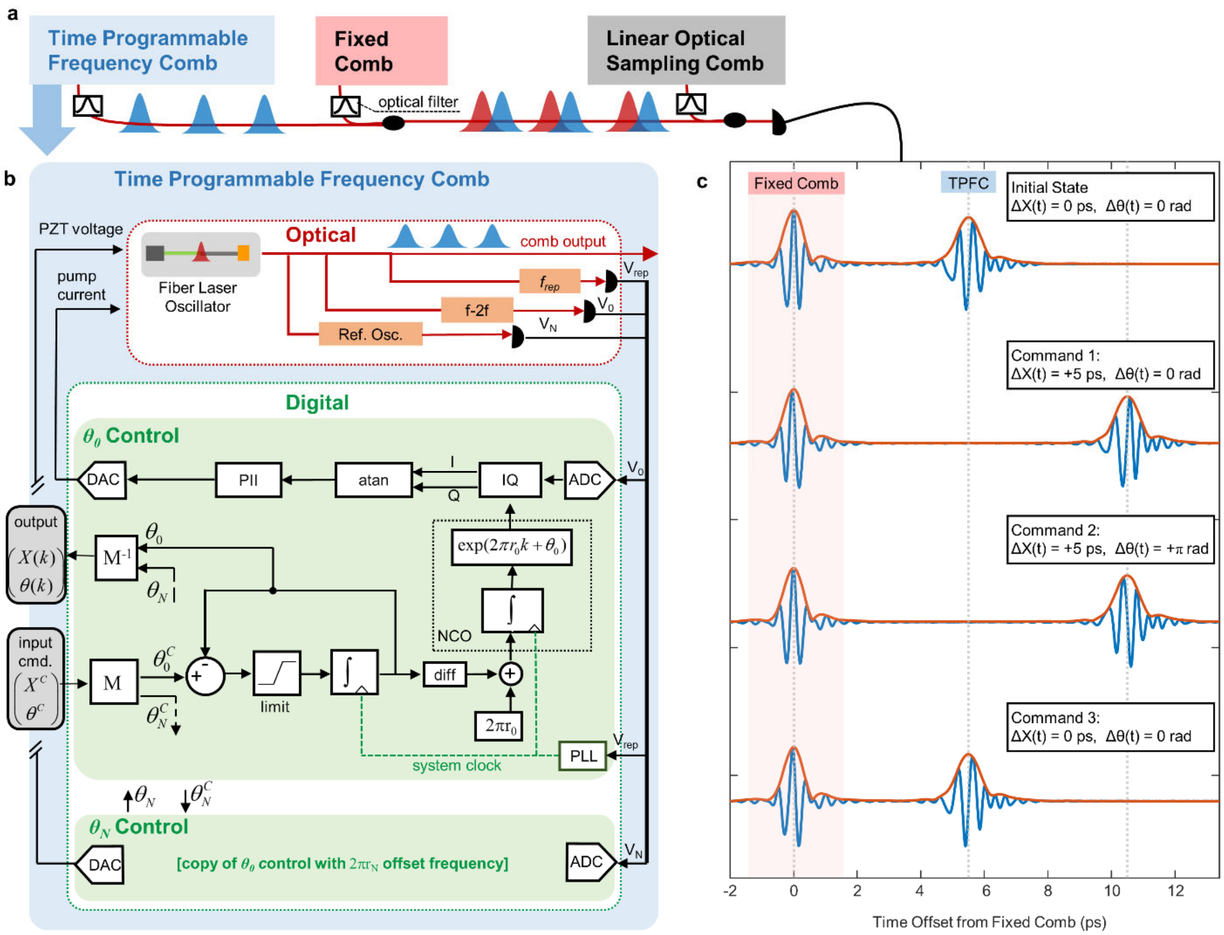

Figure 1: A time programmable frequency comb (TPFC). (a) The TPFC output is measured with respect to a second fixed frequency comb through linear optical sampling (LOS) against a third frequency comb with an offset repetition frequency. The frequency combs operate at f_{rep} ~200 MHz with a 5-ns pulse spacing. All pulses are spectrally filtered to a Gaussian 10.1-nm wide shape, corresponding to 355 fs pulse duration (See Methods). (b) Schematic of the TPFC. A self-referenced Er:fiber frequency comb is controlled with digital electronics clocked off the detected comb repetition rate signal (V_{rep}). The digital section receives the carrier-envelope offset signal (V_0), the optical beat signal (V_N), along the comb pulse timing and phase commands, X^C and θ^C, which are combined to give the control phases θ_0^C and θ_N^C through the (trivial) matrix M. These are passed to their respective digital control loop (see Methods). The control efforts for θ_0^C and θ_N^C adjust the phase-locked loops (PLLs) controlling the comb's two degrees of freedom. The system tracks the actual phases, θ_0 and θ_N as fixed point numbers, which are combined to give the actual pulse timing and phase, $X(k)$ and $\theta(k)$, for every comb pulse number k. IQ: in-phase/quadrature demodulator, PII: proportional-integral-integral controller, NCO: numerically controlled oscillator, r_0 and r_N: offset frequencies of the phase locks in units of f_{rep} (see Methods). (c) LOS (blue trace) and their envelopes (red trace) for the fixed comb (at X=0) and the TPFC at the given (X, θ) values. The LOS magnification of the time axis is 10^6.

Figures 1 and 2 describe the TPFC and its output characterization. In a self-referenced comb, phase-locked loops (PLLs) stabilize the frequency of the N^{th} comb tooth, f_N, with respect to a CW reference laser, and the frequency of the 0^{th} comb tooth, f_0 (the carrier-envelope offset frequency). The PLL locks both frequencies to a known fraction of f_{rep}, which is self-referentially defined as $f_{rep} \equiv (f_N - f_0)/N$ [1,2,4,5]. These PLLs also set the phases of the N^{th} and 0^{th} comb tooth frequencies, θ_N and θ_0, to arbitrary but fixed values. Here, we manipulate these phases to control both the comb-pulse phase, θ, and the comb-pulse time offset which is given by $X = (\theta_0 - \theta_N)/(2\pi N f_{rep})$ in direct analogy to f_{rep}'s definition above. The digital control exploits the optical frequency division of N inherent to optically self-referenced combs since a single 2π shift in the phase of either PLL leads to a time shift ~ 5 femtoseconds. The TPFC outputs both a train of optical pulses and the corresponding synchronous digital values of pulse time, X, and pulse phase, θ (Fig. 1b).

The TPFC is both agile and accurate (Figure 1c and Figure 2); the output time of a comb pulse can be adjusted arbitrarily. Yet at any instant, we know exactly, to fractions of an optical cycle, by how much the output time (and phase) has been shifted. For rapid changes in the TPFC output, the settling time of the PLLs can be taken into account either via modeling or by including the digital phase error signal from the two PLLs. It is the exactness of the performed step relative to the commanded step (Fig. 2b) and the ability to control the steps in real time that stand in contrast to earlier work. Shown in Fig. 2b, the accuracy of the timing control, *X*, with respect to the underlying CW reference laser is 0.66 ± 1.73 attoseconds.

Here the maximum slew rate between time steps was conservatively set to 40 ns/s to eliminate the possibility of cycle slips in the PLL during motion. The use of an input tracking filter for the PLL signals should enable slew rates as high as 1 μs/s, limited only by the actuators. (See Methods).

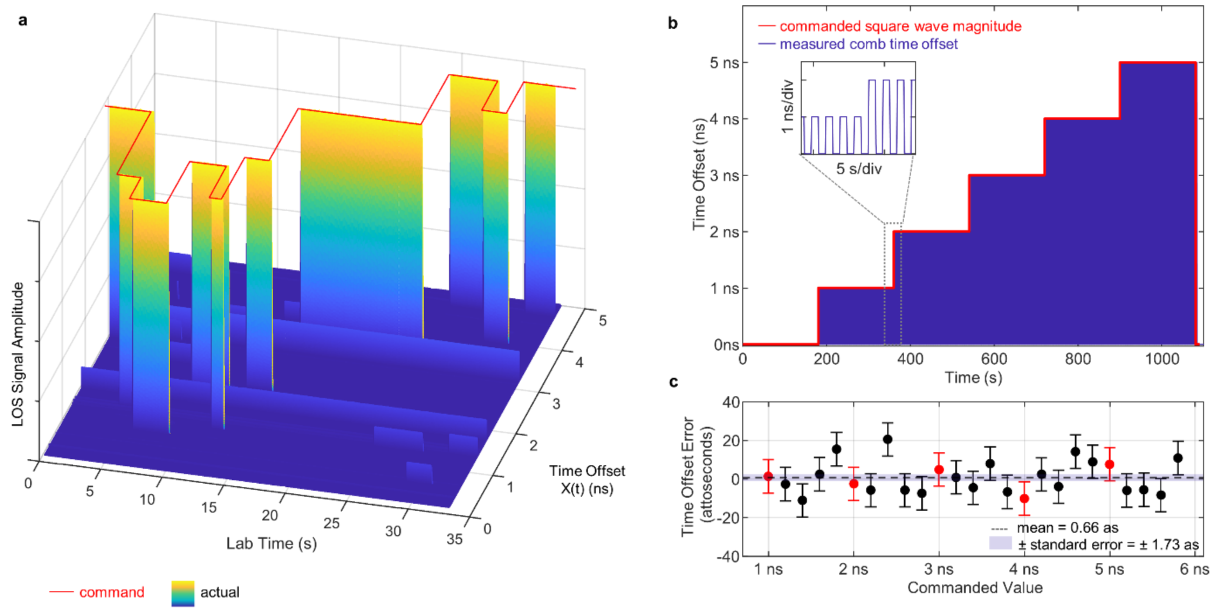

Figure 2: Illustration and characterization of the time programmability of the TPFC through LOS, using the setup in Fig 1a. (a) The TPFC pulse train, presented as a surface plot, where each slice in lab time represents a complete LOS measurement as in Figure 1c. The TPFC pulse is located at the LOS signal peak and follows the commanded arbitrary step pattern (red line). Multiple reflections within the setup appear as small satellite pulses. (b) Repeated stepping of the TPFC timing to verify accuracy. Steps are performed at 1 Hz, measured by LOS at 6 kHz (blue line), and the commanded step size (red line) is changed every 3 minutes. The 1 Hz modulation allows accurately measuring the step size by removing fiber optic path length drifts. (c) The error between the actual and commanded pulse times for the data in 2b (red circles). Each point is a 3-minute average over ~1M individual LOS measurements. This measurement was repeated for multiple different commanded time steps (black circles). The uncertainty bars are based on the LOS measurement noise and residual comb timing jitter. The average difference is 0.66 attoseconds ±1.73 attoseconds (standard error). There is no observed reduction in accuracy or precision despite moving the TPFC over the full 5 ns non-ambiguity range.

Example Application: Dual-Comb Ranging with a TPFC

To demonstrate the advantages of the TPFC in dual-comb sensing, we consider ranging[6–8]. In dual-comb ranging, pulses with bandwidth τ_p^{-1} from a comb are reflected off an object, and their time-of-flight is detected by heterodyning them against a second comb. This measurement has a resolution of $\Delta R = c\tau_p / 2$, which characterizes the ability to distinguish two adjacent reflections. It has a non-ambiguity range $R_{NA} = c / \left(2 f_{rep}\right)$, associated with "which pulse" is detected. (This ambiguity can be removed by changing f_{rep} and repeating the measurement[7]). The accuracy is set by the comb's reference oscillator or knowledge of the index of refraction. In certain applications, absolute calibration and instability of the reference plane will also factor into the accuracy. The precision is the uncertainty in the peak location of the reflection. At best, the precision is equal to the resolution divided by the signal-to-noise ratio (SNR):

$$\sigma_R = \frac{C}{2\ln(2)} \frac{\Delta R}{SNR_S} \tag{1}$$

where the $(2\ln(2))^{-1}$ factor arises from assuming Gaussian pulses (see Methods). The shot-noise limited signal-to-noise ratio, $SNR_S = \sqrt{\eta n_s}$ where η is the detector quantum efficiency and $n_s = P_{rec}T/(h\nu)$ is the number of signal photons for a received power P_{rec} and integration time, T. The constant C quantifies how far the precision is from the quantum limit. It can be related to the power penalty as $P_p = C^2$. An optimal quantum-limited ranging system operates at $C = P_p = 1$.

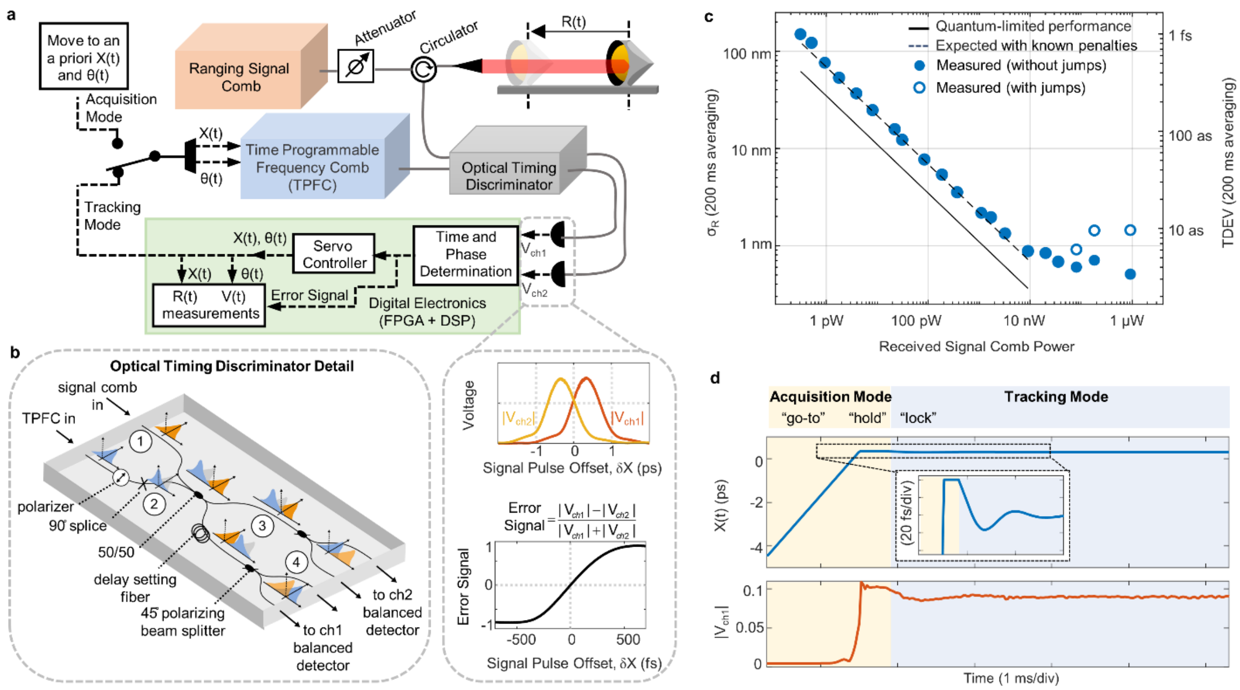

Figure 3: Dual-comb ranging with a time programmable frequency comb. (a) System diagram. The TPFC can be run in two modes, acquisition or tracking, as described in the main text. (b) The timing discriminator is a dual Mach-Zehnder interferometer constructed with polarization-maintaining fiber optics in which (1) both comb pulses enter with the same polarization and (2) the TPFC pulse is rotated to the fast-axis. Then (3) the pulses are mixed, a delay between pulses is added to one arm and (4) the pulses are projected back into the same polarization for balanced heterodyne detection to yield the two output signals V_{ch1} and V_{ch2}. These signals are demodulated and their magnitudes combined to generate a power-insensitive error signal of the differential comb pulse time offset, while their phase yields the differential comb pulse phase. (c) Range precision (deviation) σ_R (left axis) and corresponding time deviation, TDEV (right axis) at 200-ms averaging time versus the signal-comb power at the balanced photodetectors. The measured precision follows the quantum limit (Eq. (1)) from 0.33 ± 0.03 pW to 10 ± 1.0 nW with a penalty of $C = 2.16$, reaching a systematic noise floor below 1 nm (7 as), which is 2-10x below previous dual-comb ranging experiments[6–8,42–44] and attributed to residual fiber path-length fluctuations. At the three high power points, the deviation is given both for the full data trace and for a subset of the data without ~6 sudden

ranging/timing jumps of <50-nm amplitude which are attributed to nonlinear optical feedback (and only appear at these higher powers). (d) Example handover between acquisition and tracking modes. Here the TPFC was commanded to move from X(t) = -5 ps to X(t) = 0 ps where it acquires the signal pulse.

Conventional dual-comb ranging operates at a high power penalty and with significant tradeoffs. In these systems, the second comb's repetition rate is offset by Δf_r to serve as a linear sampling comb. It repeatedly scans the entire non-ambiguity range, R_{NA}, at a measurement rate $T^{-1} = \Delta f_r \leq f_{rep}\Delta R / (4R_{NA})$. The inherent tradeoffs in T, R_{NA}, and ΔR have led to dual-comb ranging implementations using very different frequency combs and covering three orders of magnitude in T and ΔR but all facing these strong constraints [6–8,42–44]. Moreover, in all cases, the power penalty $P_P \approx \Delta R / R_{NA} = f_r \tau_p$ is severe, ranging from 14 dB to 38 dB[7,42], because of the repeated scanning of the entire non-ambiguity range.

Here, as shown in Figure 3, we replace the sampling frequency comb by the TPFC to overcome these tradeoffs and stiff power penalty. A coherent timing discriminator, shown in Fig. 3b, measures the relative time and phase between the TPFC and signal comb pulses. Creating two time-shifted copies effectively shapes the TPFC pulse to optimize detection of the time of the incoming signal-comb pulses[46,47]. The two heterodyne signals output by the timing discriminator have a nominal carrier frequency of 10 MHz, set by the relative phase locks of the two combs. The signals are then bandpass filtered and demodulated. The choice of bandwidth is a tradeoff between update rate and sensitivity. Here, we use 26-kHz to be well above typical ~kHz mechanical vibrations while allowing for a fairly long 13 microsecond coherent integration time. The amplitudes of the two demodulated signals are combined to compute the time offset between the TPFC and signal comb (see Fig. 3b) while their phase yields the differential carrier phase of the TPFC and signal comb pulses whose derivative is the Doppler shift. Critically, the combination of the two channels from the timing discriminator gives a time offset measurement that is independent of the incoming signal power.

This system runs in two modes: acquisition mode and tracking mode, both of which differ from conventional dual comb ranging. In acquisition mode, X(t) is scanned until the tracking comb's timing matches the incoming signal pulse train. While it is possible to scan the entire non-ambiguity range, we can also make use of *a priori* information to scan the TPFC's over much less than the non-ambiguity range. The information could be provided from external sources or from a Kalman filter if previous range/Doppler measurements are available. Once the system acquires the appropriate reflection, it switches to tracking mode (Fig. 3d). Tracking mode implements a pulse-timing lock and a carrier-frequency lock based on the timing discriminator outputs (see Methods). The combination of the control and error signals from the time and frequency locks in turn yield the range and Doppler velocity of the target object.

In tracking mode, the ranging precision nearly reaches the quantum limit of Eq. (1) (Fig. 3c). This nearly quantum-limited precision ranging is demonstrated at a rapid 26-kHz measurement rate with as little as 0.33 ± 0.03 pW of return power ($SNR_S = 9.5$), which corresponds to only 1/77 mean photons per pulse. There is a slight penalty of $C = 2.16$x due primarily to differential dispersion between the comb pulses (see Methods). With additional optimization, C could be reduced to 1, and with squeezing, to <1 [46]. With these same 200-MHz combs, conventional dual-comb ranging would suffer from a power penalty P_p = 37 dB ($C = 71$). Finally, momentary loss of signal is not an issue. If brief enough that the object position does not differ from prediction, e.g. from a Kalman filter, by more than ~ $\pm 2\Delta R$ = ~±100 µm, tracking simply resumes. For even a 10g acceleration, a ~1.5 ms duration loss of signal is tolerable. Sometimes the signal loss may be too long, for example in strong air turbulence[48], in which case the system can transition to acquisition mode using previous data to limit the scan, as discussed above.

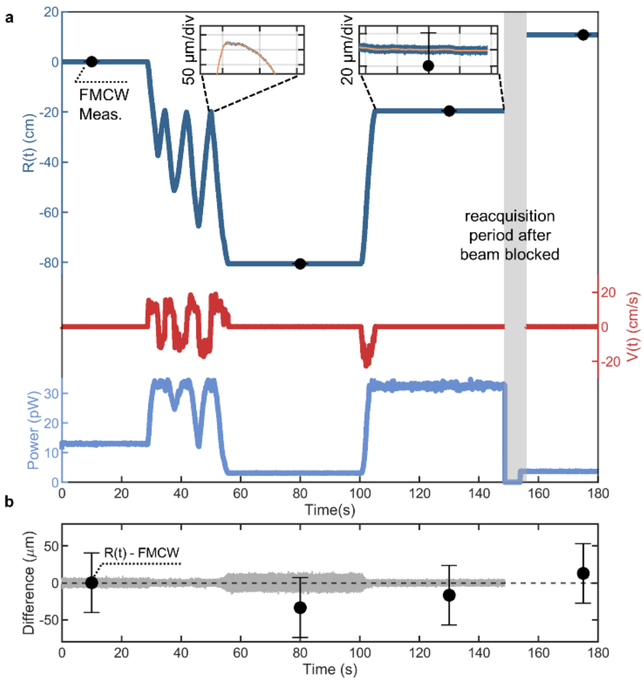

Figure 4: Ranging and velocity data to a moving retroreflector. (a) The range (top left axis, dark blue trace) is measured from the summed control and error signals for X(t) in tracking mode at a 26 kHz rate. The velocity (right middle axis, red trace) is calculated from summed control and error signals for dθ(t)/dt. At 150 seconds, the beam was blocked and the target moved, triggering a re-acquisition. Before and after re-acquisition the measured range agrees with a commercial FMCW ranging system (black circles), to within the FMCW uncertainty driven by target vibrations (see Methods). The relative range also agrees well with the interferometric range from the unwrapped carrier phase (yellow trace in the two insets), after applying an overall offset. (b) Difference between the dual-comb range and FMCW range (black circles) and between the dual-comb range and interferometric range from the unwrapped carrier phase for the initial section with continuous signal (grey trace). The range deviation of this latter difference reaches 10 nm and 5 nm at 10-s averaging for the time periods with received powers of 3.2 ± 0.3 and 32 ± 3.0 pW, respectively. (See Extended Data Figure 1.)

Figure 4 shows range data taken while moving the rail-mounted retroreflector. The dual comb system tracks the retroreflector as it reverses direction at velocities up to 20 cm/s. The signal is blocked at 150 s and the retroreflector moved, after which the absolute range was reacquired by scanning over a ±37.5 cm window. For validation, we compare to a commercial frequency-modulated continuous-wave (FMCW) system at a few static rail positions after calibrating out differential range offsets. The two agree to within the FMCW measurement uncertainty of ±40 µm due to target vibrations amplified by the FMCW's intrinsic range-doppler coupling (Extended Data Figure 2). Finally, the coherent timing discriminator also outputs the relative carrier phase between the signal comb and TPFC, whose derivative yielded the velocity above. This phase can also be unwrapped to provide relative range during periods of continuous signal (Fig. 4, yellow trace) as in Ref. [7] and similar to CW interferometry (except avoiding systematic errors from spurious reflections). This unwrapped carrier phase agrees with the tracking range to a precision limited by the tracking range noise which follows Eq. (1), after accounting for a ~1.5x chirp-induced penalty in *C* from the fiber optic path to reach the rail system.

DISCUSSION

A number of existing or potential applications should benefit from the abilities illustrated in Fig. 1-3, specifically to (1) set the time and phase of the comb's output pulses, (2) coherently scan the relative temporal spacing between two frequency combs over a specified limited range rather than the full inverse repetition rate, thereby mimicking a higher repetition-rate comb while avoiding limitations of lower pulse energy, and (3) operate as a precision optical tracking oscillator in time and frequency for shot-noise limited sensing. Below we discuss three different general application areas: LIDAR, time metrology, and spectroscopic sensing.

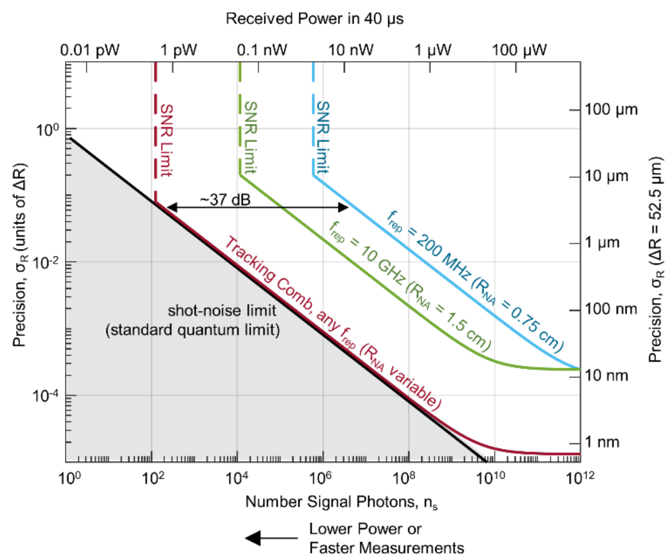

Figure 5: Precision versus received signal photons, $n_S = SNR_S^2/\eta$, for conventional dual-comb ranging at f_{rep} = 200 MHz (blue line) and f_{rep} = 10 GHz (green line), compared to tracking dual-comb ranging (red line) and the standard quantum limit for heterodyne detection (black line). The left/bottom axes are in normalized units while the right/top axes are scaled to values similar to those used in this work. For conventional dual-comb ranging, the scaling depends strongly on f_{rep} and the precision is always much worse than the standard quantum limit. The tracking dual-comb ranging (red line) is independent of f_{rep} and can reach the standard quantum limit, though here shown with a 10% penalty. We assume a system noise floor of 0.7 nm, taken from this work, for the tracking comb, and ~10 nm for the conventional dual-comb systems[7,42]. For all three ranging configurations, we require a minimum detection SNR of ~10 for reasonable detection statistics, as indicated by the SNR limit. The 37 dB improvement, however, is independent of this chosen limit.

As already discussed, frequency combs have a natural connection to precision LIDAR. Figure 5 and Extended Data Table 1 together compare conventional dual-comb ranging[7,42–44], tracking dual-comb ranging and FMCW ranging[49], which is the standard approach to high-resolution optical ranging. For all three, the resolution is set by the optical bandwidth and the accuracy by the comb referencing or knowledge of the index of refraction of air. (Comb-assisted FMCW ranging can transfer frequency-comb accuracy to FMCW LIDAR[50].) Both tracking dual-comb ranging and FMCW ranging can reach the shot-noise limit and exploit the optical carrier phase. However, the update rate of FMCW ranging is limited by the laser sweep time and its uncertainty can be degraded by target vibrations. Tracking dual-comb ranging avoids vibration-related systematics. It could provide range-resolved vibrometry in a cluttered environment or surface imaging through turbulent media even with speckle-induced dropouts and high loss. (A 10-mW launch power will still provide sufficient 1-pW return power to enable a 26-kHz measurement rate given a -100 dB reflection). More generally, there are strong overlaps with conventional RF pulse-Doppler radar and the tracking comb could therefore have interesting applications to high-bandwidth synthetic aperture LIDAR[51].

In time-frequency metrology, a TPFC phase-locked to an optical atomic clock provides an optical timescale with the ability to “adjust” its output time to synchronize with other signals. A TPFC could also enable calibration of time interval counters[45]. The time-interval standard would follow Fig. 1c, where the TPFC allows precisely defined variable pulse spacing from nanoseconds to femtoseconds. This offers the prospect of a time interval standard that spans 6 orders of magnitude with attosecond precision and an accuracy directly tied to a secondary representation of the second. For absolute optical frequency measurements, the TPFC also enables determination of the mode number N by applying a shift $\Delta\theta_0 = 2\pi N$, which will lead to a time shift of exactly $\Delta X = f_{rep}^{-1}$ for the correct N. Any integer error in N appears as a multiple of 5-fs offset in time, which can be resolved with a second comb and a timing discriminator. In secure optical communications, the programmable comb might enable quadrature pulse phase-position modulation if implemented with high-speed actuators. Finally, the TPFC has interesting applications to comb-based long-distance free-space time transfer [13–17,19,20,23,48] as it provides similar advantages as in dual-comb ranging[52].

The TPFC can also break tradeoffs that limit comb-based linear and non-linear spectroscopy. Relatively low repetition-rate frequency combs (100-MHz to 1-GHz) provide the high pulse energies needed for nonlinear spectroscopy or for spectrally broadening over the desired spectral band[53–55]. However, the spectral resolution set by these low repetition rates is often poorly matched to the application leading to significant “deadtime” or SNR reduction in multi-comb-based spectroscopy[24,26–31,54,55]. The TPFC can circumvent this problem by coherently scanning over a limited time offset between two or more frequency combs, as first demonstrated incoherently in the early dual-comb spectroscopic work of Schliesser *et al.*[38]. In this way, a low-repetition frequency TPFC can act as a frequency comb with an effectively much higher repetition rate, set by the inverse of the temporal scan window, at shot-noise limited sensitivity. Going further, the ability to jump the frequency comb pulse phase and timing could enable compressive sampling in dual-comb or multi-comb sensing applications with a concomitant increase in measurement rate. Recent modeling[35] and preliminary experiments[34] have highlighted the advantages of this dynamic control for dual-comb spectroscopy. Finally, in nonlinear spectroscopy, temporal control could enable time-ordered multi-photon excitation, following the comb-based spectroscopy of Rubidium[33] but with programmable control.

CONCLUSION

The time programmable frequency comb combines the precision and accuracy of a self-referenced frequency comb with flexibility in time and phase and 2-attosecond accuracy. Here, the TPFC is based on a fiber frequency comb, but any self-referenced comb (or comb locked to widely separated optical oscillators) with control electronics capable of tracking and manipulating phase could act as a TPFC. Through a dual-comb ranging demonstration, we show the TPFC can operate as an optical tracking oscillator in time and frequency, yielding nearly quantum-noise limited ranging with 0.7 nm precision. Finally, dual-comb ranging is just one application and the TPFC has equal promise in relaxing tradeoffs with repetition frequency and improving SNR in other multi-comb sensing and metrology applications while retaining the hallmark accuracy of comb-based metrology.

ACKNOWLEDGMENTS

We acknowledge Jennifer Ellis, Tara Fortier, Kevin Cossel, William Swann, Benjamin Stuhl, and Brian Washburn for helpful discussions.

AUTHOR CONTRIBUTIONS

All authors contributed extensively to this work.

COMPETING INTERESTS

The authors declare no competing interests.

DATA AVAILABILITY

The data for the figures in this manuscript are available for download at https://data.nist.gov/sdp/<to be provided>/.

CODE AVAILABILITY

The mathematics and algorithms necessary to create a time programmable frequency comb are described between the main text and the methods section.

MATERIALS AND CORRESPONDANCE

Should be addressed to Laura Sinclair (laura.sinclair@nist.gov) or Nathan Newbury (nathan.newbury@nist.gov).

REFERENCES

1. Hänsch, T. W. Nobel Lecture: Passion for precision. *Rev. Mod. Phys.* **78**, 1297–1309 (2006).
2. Hall, J. L. Nobel Lecture: Defining and measuring optical frequencies. *Rev. Mod. Phys.* **78**, 1279–1295 (2006).

3. Newbury, N. R. Searching for applications with a fine-tooth comb. *Nat. Photon* **5**, 186–188 (2011).
4. Fortier, T. & Baumann, E. 20 years of developments in optical frequency comb technology and applications. *Commun. Phys.* **2**, 1–16 (2019).
5. Diddams, S. A., Vahala, K. & Udem, T. Optical frequency combs: Coherently uniting the electromagnetic spectrum. *Science* **369**, eaay3676 (2020).
6. Zhu, Z. & Wu, G. Dual-Comb Ranging. *Engineering* **4**, 772–778 (2018).
7. Coddington, I., Swann, W. C., Nenadovic, L. & Newbury, N. R. Rapid and precise absolute distance measurements at long range. *Nat. Photon* **3**, 351–356 (2009).
8. Kim, W. *et al.* Absolute laser ranging by time-of-flight measurement of ultrashort light pulses [Invited]. *JOSA A* **37**, B27–B35 (2020).
9. Minoshima, K. & Matsumoto, H. High-accuracy measurement of 240-m distance in an optical tunnel by use of a compact femtosecond laser. *Appl Opt* **39**, 5512–5517 (2000).
10. Vicentini, E., Wang, Z., Van Gasse, K., Hänsch, T. W. & Picqué, N. Dual-comb hyperspectral digital holography. *Nat. Photonics* **15**, 890–894 (2021).
11. Kato, T., Uchida, M. & Minoshima, K. No-scanning 3D measurement method using ultrafast dimensional conversion with a chirped optical frequency comb. *Sci. Rep.* **7**, 3670 (2017).
12. Hase, E. *et al.* Scan-less confocal phase imaging based on dual-comb microscopy. *Optica* **5**, 634–643 (2018).
13. Deschênes, J.-D. *et al.* Synchronization of Distant Optical Clocks at the Femtosecond Level. *Phys. Rev. X* **6**, 021016 (2016).
14. Giorgetta, F. R. *et al.* Optical two-way time and frequency transfer over free space. *Nat. Photonics* **7**, 434–438 (2013).

15. Xin, M., Şafak, K. & Kärtner, F. X. Ultra-precise timing and synchronization for large-scale scientific instruments. *Optica* **5**, 1564–1578 (2018).

16. Shen, Q. *et al.* Experimental simulation of time and frequency transfer via an optical satellite–ground link at 10^{-18} instability. *Optica* **8**, 471–476 (2021).

17. Boulder Atomic Clock Optical Network (BACON) Collaboration *et al.* Frequency ratio measurements at 18-digit accuracy using an optical clock network. *Nature* **591**, 564–569 (2021).

18. Clivati, C. *et al.* Common-clock very long baseline interferometry using a coherent optical fiber link. *Optica* **7**, 1031–1037 (2020).

19. Bergeron, H. *et al.* Femtosecond time synchronization of optical clocks off of a flying quadcopter. *Nat. Commun.* **10**, 1819 (2019).

20. Bodine, M. I. *et al.* Optical time-frequency transfer across a free-space, three-node network. *APL Photonics* **5**, 076113 (2020).

21. Dix-Matthews, B. P. *et al.* Point-to-point stabilized optical frequency transfer with active optics. *Nat. Commun.* **12**, 515 (2021).

22. Gozzard, D. R. *et al.* Ultrastable Free-Space Laser Links for a Global Network of Optical Atomic Clocks. *Phys. Rev. Lett.* **128**, 020801 (2022).

23. Shen, Q. *et al.* 113 km Free-Space Time-Frequency Dissemination at the 19th Decimal Instability. *ArXiv220311272 Phys.* (2022).

24. Coddington, I., Newbury, N. & Swann, W. Dual-comb spectroscopy. *Optica* **3**, 414–426 (2016).

25. Cossel, K. C. *et al.* 2 - Remote sensing using open-path dual-comb spectroscopy. in *Advances in Spectroscopic Monitoring of the Atmosphere* (eds. Chen, W., Venables, D. S. & Sigrist, M. W.) 27–93 (Elsevier, 2021). doi:10.1016/B978-0-12-815014-6.00008-7.
26. Picqué, N. & Hänsch, T. W. Frequency comb spectroscopy. *Nat. Photonics* **13**, 146–157 (2019).
27. Lomsadze, B., Smith, B. C. & Cundiff, S. T. Tri-comb spectroscopy. *Nat. Photonics* **12**, 676–680 (2018).
28. Friedlein, J. T. *et al.* Dual-comb photoacoustic spectroscopy. *Nat. Commun.* **11**, 3152 (2020).
29. Wildi, T., Voumard, T., Brasch, V., Yilmaz, G. & Herr, T. Photo-acoustic dual-frequency comb spectroscopy. *Nat. Commun.* **11**, 4164 (2020).
30. Ideguchi, T. *et al.* Coherent Raman spectro-imaging with laser frequency combs. *Nature* **502**, 355–358 (2013).
31. Rieker, G. B. *et al.* Frequency-comb-based remote sensing of greenhouse gases over kilometer air paths. *Optica* **1**, 290–298 (2014).
32. Voumard, T. *et al.* AI-enabled real-time dual-comb molecular fingerprint imaging. *Opt. Lett.* **45**, 6583–6586 (2020).
33. Marian, A., Stowe, M. C., Lawall, J. R., Felinto, D. & Ye, J. United Time-Frequency Spectroscopy for Dynamics and Global Structure. *Science* **306**, 2063–2068 (2004).
34. Giorgetta, F. R. *et al.* Fiber Laser Based Dual-Comb Spectroscopy with Dynamically Controlled Spectral Resolution. in *Conference on Lasers and Electro-Optics (2021), paper AM3E.4* AM3E.4 (Optical Society of America, 2021).
35. Kawai, A., Kageyama, T., Horisaki, R. & Ideguchi, T. Compressive dual-comb spectroscopy. *Sci. Rep.* **11**, 13494 (2021).

36. Martin, B., Feneyrou, P., Dolfi, D. & Martin, A. Performance and limitations of dual-comb based ranging systems. *Opt. Express* **30**, 4005 (2022).

37. Ellis, J. L. *et al.* Scaling up Frequency-Comb-Based Optical Time Transfer to Long Terrestrial Distances. *Phys. Rev. Appl.* **15**, 034002 (2021).

38. Schliesser, A., Brehm, M., Keilmann, F. & van der Weide, D. Frequency-comb infrared spectrometer for rapid, remote chemical sensing. *Opt. Express* **13**, 9029–9038 (2005).

39. Tourigny-Plante, A., Guay, P. & Genest, J. Apodization in dual-comb spectroscopy for rapid measurement. in *Optical Sensors and Sensing Congress (2020), paper LTu3C.2* LTu3C.2 (Optical Society of America, 2020).

40. Shi, Y. *et al.* High speed time-of-flight displacement measurement based on dual-comb electronically controlled optical sampling. *Opt. Express* **30**, 8391–8398 (2022).

41. Antonucci, L., Solinas, X., Bonvalet, A. & Joffre, M. Asynchronous optical sampling with arbitrary detuning between laser repetition rates. *Opt. Express* **20**, 17928–17937 (2012).

42. Trocha, P. *et al.* Ultrafast optical ranging using microresonator soliton frequency combs. *Science* **359**, 887–891 (2018).

43. Mitchell, T., Sun, J., Sun, J. & Reid, D. T. Dynamic measurements at up to 130-kHz sampling rates using Ti:sapphire dual-comb distance metrology. *Opt. Express* **29**, 42119–42126 (2021).

44. Suh, M.-G. & Vahala, K. J. Soliton microcomb range measurement. *Science* **359**, 884–887 (2018).

45. Kalisz, J. Review of methods for time interval measurements with picosecond resolution. *Metrologia* **41**, 17–32 (2004).

46. Fabre, C. & Treps, N. Modes and states in quantum optics. *Rev. Mod. Phys.* **92**, 035005 (2020).

47. Ansari, V. *et al.* Achieving the Ultimate Quantum Timing Resolution. *PRX Quantum* **2**, 010301 (2021).

48. Sinclair, L. C. *et al.* Synchronization of clocks through 12 km of strongly turbulent air over a city. *Appl. Phys. Lett.* **109**, 151104 (2016).

49. Barber, Z. W., Dahl, J. R., Sharpe, T. L. & Erkmen, B. I. Shot noise statistics and information theory of sensitivity limits in frequency-modulated continuous-wave ladar. *J. Opt. Soc. Am. A* **30**, 1335–1341 (2013).

50. Baumann, E. *et al.* Comb-calibrated frequency-modulated continuous-wave ladar for absolute distance measurements. *Opt. Lett.* **38**, 2026–2028 (2013).

51. Crouch, S. & Barber, Z. W. Laboratory demonstrations of interferometric and spotlight synthetic aperture ladar techniques. *Opt Express* **20**, 24237 (2012).

52. Caldwell, E. D. *et al.* Photon Efficient Optical Time Transfer. in *Proc. IFCS-EFTF* vol. 2022 (2022).

53. Schliesser, A., Picqué, N. & Hänsch, T. W. Mid-infrared frequency combs. *Nat. Photonics* **6**, 440–449 (2012).

54. Ycas, G. *et al.* High-coherence mid-infrared dual-comb spectroscopy spanning 2.6 to 5.2 µm. *Nat. Photonics* **12**, 202–208 (2018).

55. Muraviev, A. V., Smolski, V. O., Loparo, Z. E. & Vodopyanov, K. L. Massively parallel sensing of trace molecules and their isotopologues with broadband subharmonic mid-infrared frequency combs. *Nat. Photonics* **12**, 209–214 (2018).